



OPEN Implementing a novel TOPSIS-sine cosine algorithm-based hybrid optimization in machining medium-hardened steel

Ramanuj Kumar¹, Mohammad Rafighi^{2,3}, Oğur İynen⁴, M. Prem Kumar Reddy⁵, Shrikant Zade⁶, Mustafa Özdemir⁷, Anish Pandey¹✉ & Ramanpreet Singh⁸✉

Machining medium-hardened steel is particularly challenging because of its high strength and wear resistance, which generate excessive cutting temperatures. The elevated temperature contributes to rapid tool wear and negatively impacts surface quality. Optimizing tool selection, coating composition, geometry, and process variables is crucial for enhancing machinability. This study applied a novel hybrid TOPSIS-sine cosine algorithm to evaluate the performance of three chemical vapor deposited (CVD)-coated carbide cutting inserts in turning medium-hard AISI 4340 grade steel, considering the depth of cut (a), cutting speed (V), feed (f) and workpiece hardness as input variables. Experimentally obtained machining responses, namely resultant force (F_r), power consumption (P_c), surface roughness (R_a), and sound level (SL), were analyzed and compared to determine the optimum insert type. Insert type-3 (TiCN-Al₂O₃-TiN) demonstrated superior performance, achieving a 16.68% and 26.74% lower R_a than insert type-1 and type-2, respectively. Moreover, the optimal parameters for the most favorable insert (type-3) are determined as $H = 30$ HRC, $V = 190$ m/min, $f = 0.1$ mm/rev, and $a = 0.2$ mm. Workpiece hardness (H) emerged as the most influential factor affecting machining outcomes. This research recommended insert type-3 at optimized cutting conditions to improve machinability and sustainability in turning medium-hard AISI 4340 grade steel.

Keywords Coated carbide tools, Medium hardened steel, Turning, TOPSIS-sine cosine algorithm, Surface roughness, Cutting forces

Abbreviations

a	Depth of cut, mm
AISI	American iron and steel institute
CBN	Cubic boron nitride
CNC	Computer numerical control
CVD	Chemical vapor deposition
f	Feed rate
I	Current
MRR	Material removal rate
P_c	Power consumption
PCBN	Polycrystalline cubic boron nitride
PVD	Physical vapor deposition
V	Cutting speed

¹School of Mechanical Engineering, Kalinga Institute of Industrial Technology (KIIT), Deemed to Be University, Bhubaneswar, Odisha 751024, India. ²Department of Mechanical Engineering, Başkent University, Ankara 06490, Türkiye. ³School of Mechanical Engineering, Purdue University, West Lafayette, IN 47907, USA. ⁴Department of Mechanical Engineering, Yozgat Bozok University, 66100 Yozgat, Türkiye. ⁵Department of Mechanical Engineering, Aditya University, Surampalem, Andhra Pradesh 533437, India. ⁶Department of Computer Science Engineering, Nagpur Institute of Technology, Nagpur, Maharashtra 440013, India. ⁷Department of Machine and Metal Technology, Yozgat Bozok University, 66100 Yozgat, Türkiye. ⁸Department of Mechanical Engineering, Manipal University Jaipur, Jaipur, Rajasthan 303007, India. ✉email: anish.pandeyfme@kiit.ac.in; ramanpreet.singh@jaipur.manipal.edu

<i>TiN</i>	Titanium nitride
<i>AlCrN</i>	Aluminium chromium nitride
<i>Al₂O₃</i>	Aluminium oxide
<i>TiAlN</i>	Titanium aluminium nitride
<i>ZrCN</i>	Zirconium carbo-nitride
<i>Ra</i>	Average surface roughness
<i>Rq</i>	Root mean square
<i>Rz</i>	Peak-to-valley height
<i>HRC</i>	Rockwell hardness in C scale
<i>H</i>	Workpiece hardness
<i>F_x</i>	Radial force
<i>F_y</i>	Feed force
<i>F_z</i>	Cutting force
<i>F_r</i>	Resultant force
<i>SCA</i>	Sine cosine algorithm
<i>rpm</i>	Revolution per minute
<i>SL</i>	Sound level
<i>TOPSIS</i>	Technique for order preference by similarity to ideal solution
<i>Volt.</i>	Voltage
<i>TiC</i>	Titanium carbide
<i>TiSiN</i>	Titanium silicon nitride
<i>TiCN</i>	Titanium carbide nitride

Hard turning serves as an effective alternative to grinding, making it especially valuable in industries such as die-mold, automotive, and bearing industries^{1,2}. It provides many advantages, such as an environmentally friendly process due to the elimination of cutting fluid, shorter cycle time, lower manufacturing cost, and energy consumption^{3,4}. In the hard turning process, a specified layer of heat-treated steel chip is machined from the specimen with a sharp edge of a single-point cutting edge through plastic deformation, followed by the shearing phenomenon⁵. According to the literature, severe tool wear, higher turning forces, and greater temperature are the significant limitations of hard turning^{6,7}. In some studies, different cooling conditions were used to lower the temperature of both the job and the turning tool, which leads to longer tool life^{8,9}. The use of coolant is expensive, and it has many ecological issues for both operator safety and the environment. Therefore, dry-cutting conditions are used by numerous researchers who consider relevant cutting tools and cutting conditions^{10,11}.

When machining hardened steels, the exceptionally hard tool materials, including polycrystalline boron nitride (PCBN) and cubic boron nitride (CBN), deliver good surface quality and dimensional precision due to their excellent properties under raised temperatures and higher machining speeds^{12–14}. These cutting tools have excellent wear resistance, outstanding thermo-mechanical stability, and good hardness. These tools are superbly suited for hard turning, but they are expensive and lead to high production costs.

The machinability of a particular material is affected by many factors. According to previous studies^{15–18}, the most critical factors influencing machinability are cutting parameters, hardness of test workpiece, tool designation, and tool materials. Recently, most researchers have focused on using economic cutting tools such as coated carbide in machining hard steel to reduce production costs^{19–22}. The enactment of coated carbide cutting tools mostly depends on coating types, tool geometry, and machining parameters. Many scholars have applied different coatings on the carbide substrate to improve heat evacuation, decrease tool wear and abrasion resistance, and minimize friction between the cutting tool and test workpiece^{23,24}. The coating material functions as a thermal and chemical barrier, which reduces chemical reactions and diffusion between the machining tool and test workpiece²⁵. However, when the coated cutting tool is used to machine the material at a low speed, it is prone to peeling and chipping, making it unsuitable for low-speed cutting scenarios²⁶. The coating procedure has a considerable consequence on the cutting competencies of the coated tool. Chemical vapor deposition (CVD) and physical vapor deposition (PVD) are widely recognized techniques for depositing layers on carbide substrates⁹. According to the literature, the most commonly used coatings on the carbide substrate for machining hard steel are TiN/AlCrN²⁷, Al₂O₃/TiC^{27,28}, TiSiN/TiAlN^{29,30}, TiAlN/TiN^{31,32}, Al₂O₃/TiCN³³, TiN/Al₂O₃/TiCN³⁴, TiN/TiAlN/TiC³⁵, TiN/TiCN/Al₂O₃^{36,37}, TiC/TiCN/Al₂O₃³⁸, TiCN/Al₂O₃/TiN^{39,40}, TiN/TiCN/Al₂O₃/TiN^{41,42}, TiN/TiCN/Al₂O₃/ZrCN⁴³, and TiC/TiCN/Al₂O₃/TiN⁴⁴. Here are some advantages of the coatings mentioned above: Al₂O₃: excellent crater resistance, TiC: excellent wear resistance, TiN: excellent built-up edge resistance, TiCN: harder than TiN, TiAlN: harder than other PVD coating types. The comparative performance of these coatings is rarely listed in the literature. Therefore, it is noteworthy to consider this aspect for the better applicability of coated tools in turning hardened steel.

The following literature study critically examines the effectiveness of various coating tools in turning AISI 4340 hard grade steel: Das et al.¹⁹ studied the consequence of cutting variables on the chip morphology, surface roughness, and tool wear when using a CVD make coating tool (TiN/TiCN/Al₂O₃/TiN). According to the results, feed and cutting speed significantly impacted wear and roughness, respectively. Finally, the SEM demonstrates that abrasion is the coated carbide tool's principal wear mechanism. Suresh et al.³⁸ performed hard turning using CVD-coating (TiC/TiCN/Al₂O₃) tool. The results reported that the highest speed with low feed and low cutting depth minimizes the machining force and roughness. In contrast, wear and machining power improved with larger feed and greater cutting speed. Das et al.⁴¹ observed that tool feed and machining speed significantly influence surface quality and tool wear. Chinchankar and Choudhury⁴² compared the performance of CVD (TiCN/Al₂O₃/TiN) and PVD (TiAlN) coated tools in turning AISI 4340 grade steel. Improved surface quality and lower cutting force are achieved using the CVD coating tool compared to the PVD coating tool. Awadh

et al.⁴⁵ monitored that the TiAlSiN-coated tool outperformed TiCN/Al₂O₃/TiN and TiAlN/TiN-coating tools in cutting AISI 4340 grade steel. The TiCN/Al₂O₃/TiN tool resulted in 32% more roughness than the TiAlN/TiN tool and 69% more than the TiAlSiN tool. Butt et al.⁴⁶ compared the CVD- and PVD-tool performance for cutting AISI 4340 grade steel, evaluating roughness and tool flank wear as machinability criteria. Feed rate had the maximum impact on roughness, followed by speed. PVD tool achieved improved surface smoothness at lower speeds, while CVD tool performed similarly at elevated speeds. Additionally, CVD tool exhibited lower wear than PVD tool.

Cutting tool geometry is crucial for machining performance. Duc et al.⁴⁷ examined the influence of rake angle, cutting edge angle, and inclination angle on tool wear, and surface roughness in machining AISI 1055 grade heat-treated steel with ceramic (TiN coating) inserts. Their findings highlighted the inclination angles as the most relevant angle affecting both tool wear and surface quality. Azaath et al.⁴⁸ investigated tool geometry's impact in cutting AISI 4340 grade steel with finite element analysis. According to the results, microgroove cutting tools have a minimum wear rate compared to other cutting tools with different geometries. In addition, the cutting tool interface temperature is reduced with the microgroove tool; it was increased while using the zero-degree rake angle tool. According to Dogra et al.⁴⁹, chip breaker geometry greatly affects the machining process. Chip breaker geometry directly affects the consequence of restricted contact length and significantly affects the wear, cutting forces, and surface roughness in machining.

In addition, workpiece properties and cutting parameters affect the machinability criteria. Kambagowni et al.⁵⁰ examined the impact of workpiece hardness in machining AISI 4340 grade steel, considering three distinct hardness levels (45, 50, and 55 HRC). Based on the results, feed rate had the most significant consequence on the Ra, Rq, and Rz, while hardness had the greatest impact on the Rt. Chinchanihar and Choudhury⁵¹ investigated how cutting input terms and tool coating (CVD-TiCN/Al₂O₃/TiN and PVD-TiAlN) affect temperature in machining heat-treated AISI 4340 grade steel. Their findings revealed that the CVD coating tool produces higher interface temperatures than PVD. Chinchanihar and Choudhury⁵² discovered that using lower feed and lower depth of cut while turning medium-hardened steel with 144 m/min of speed resulted in reduced forces, improved surface quality, and extended tool life. Ji et al.⁵³ investigated the performance of silicone carbide ceramic in the end electric discharge machine (EDM). They tried to minimize machining cost and surface roughness while machining a large surface area on SiC ceramic. The findings showed that SiC ceramic is eliminated by employing melting, evaporation, and thermal spalling. Additionally, material from the tool electrode may be transferred to the workpiece, resulting in a reaction during the electric discharge milling process of the SiC ceramic. Chi et al. presented laser-assisted milling (LAM) on the γ -TiAl alloy to evaluate its surface integrity and machinability⁵⁴. The results show that LAM can significantly improve surface integrity and decrease the cutting forces of the specimen.

In machining research, multi-response optimization is highly essential to achieving high productivity. In the past, many conventional and algorithmic optimization methods have been applied in hard-turning studies. Recently, the integration of conventional and algorithm-based optimization techniques has gained popularity, utilizing the benefits of both approaches. The implementation of stochastic algorithms alone can be found in many areas of science and technology because these algorithms help us find optimal or near-optimum input and output values from the given data set. Therefore, researchers have developed various stochastic optimization algorithms^{55,56} inspired by different phenomena^{57,58}, like swarm-based, e.g., particle swarm algorithm, physics-based⁵⁹, e.g., wind-driven optimization algorithm, and evolutionary-grounded^{60,61}, e.g., genetic algorithm. However, each algorithm has pros and cons based on its computational complexity and performance⁶². Most algorithms are applied to solve various engineering and structural problems⁶³. Based on the performance evaluation of different optimization algorithms with the Sine Cosine Algorithm (SCA) reported in an article⁶². In the current research, the SCA was chosen to implement with the standard TOPSIS (Technique for Order of Preference by Similarity to Ideal Solution) approach for searching optimal or near-optimum rates of different machining constraints. Some more work related to implementing optimization algorithms in machining and other applications is reported in articles⁶⁴⁻⁶⁸.

According to the literature, several investigations have been conducted on the machining properties of AISI 4340 steel using PVD- or CVD-coating tools. The machining evaluation of medium hardened AISI 4340 grade steel utilizing three distinct coated carbide cutting tools has not yet been tested; nevertheless, these innovative works are being considered in the current research. Furthermore, relatively few researchers have investigated the machinability of AISI 4340 steel by utilizing cutting sound as a performance metric. This study used the sound level as a performance measure to compare and explore the machinability of AISI 4340 steel. Furthermore, a novel hybrid optimization technique known as the TOPSIS-Sine Cosine algorithm was devoted to optimizing the process variables to increase productivity and sustainability. Moreover, carbon emission was also estimated at optimal cutting conditions to compare the performance among these tools, which is another innovative study for green manufacturing concerns. Overall, the key goal of this study is to determine the most effective cutting tool and input parameter values to boost the machinability of medium-hardened steel for industrial applications.

Materials and methods

Workpiece properties and heat treatment

AISI 4340 steel is provided as a cylindrical extruded bar measuring 38 mm in diameter and 250 mm in length. The Thermo-Scientific ARL PERFORM'X XRF Sequential X-Ray device is utilized to estimate the chemical components of the tested sample. The chemical composition (% of weight) of the tested sample was found as follows: P = 0.02, Mg = 0.05, Si = 0.18, Mo = 0.19, C = 0.35, Mn = 0.58, Ni = 1.48, Cr = 1.58, and Fe (balance).

Firstly, cylindrical bars (38 mm in diameter and 250 mm in length) underwent normalization to enhance ductility and toughness while eliminating dendritic segregation from the casting. The materials were then

annealed at 840 °C for 1.5 h in an atmosphere-controlled furnace, followed by air cooling at ambient temperature (approximately 20 °C for 5 h). As a result, the specimens achieved a hardness of 38 ± 1 HRC.

Then, the samples were austenitized at 860 °C for 90 min utilizing an atmosphere-controlled furnace to obtain different quenched and tempered martensite structures. After this, it was left to cool in oil (about 20 °C and 5 h). Hence, the hardness of the specimens reached 55 ± 1 HRC. Finally, the specimens were kept constant at 510 °C, 560 °C, and 610 °C for 1.5 h, utilizing a tempering furnace to perform a quenched martensite structure, respectively. Also, the furnace temperature was intensified at a heating rate of 70–75 °C/h. All other specimens were cooled in still air at ambient temperature, about 20 °C, for 5 h. As a result of this, specimens with 40 ± 1 HRC, 35 ± 1 HRC, and 30 ± 1 HRC hardness were obtained, respectively. A schematic illustration of the heat cycle for quenching and tempering of AISI 4340 grade steel is given in Fig. 1.

Cutting inserts and tool holder

The experiments were executed using three cutting inserts: insert type-1: Kennametal CNMG 120408 MP, insert type-2: Kennametal CNMG 120408 RP, and insert type-3: Walter CNMG 120408 NM4. Table 1 provides details of the inserts and tool holder.

Measurement of cutting force

KISTLER 9129AA piezoelectric dynamometer was utilized to measure the cutting forces. It is capable of measuring the cutting force in the range of ± 10 kN, with sampling frequency of F_x : 3.5 kHz, F_y : 4.5 kHz, F_z : 3.5 kHz and sensitivity of F_x : -8 pC/N, F_y : -4.1 pC/N, F_z : -8 pC/N. The dynamometer calibration was done before the actual measurement, and the calibration standard error was within $\pm 3\%$. A Kistler 3-component piezoelectric dynamometer provides the measurement of machining force that measures averaged F_x : radial force, F_y : feed force, and F_z : tangential force in turning processes. Similar methodology was used by many authors⁴⁵. Moreover, the resultant force (F_r) was estimated by taking the square root of $(F_x^2 + F_y^2 + F_z^2)$. Data Acquisition Card and Dynaware software were used to record graphical displays of force results. The force measurement experimental setup is presented in Fig. 2. The experiments were executed three times, and the experimental standard error for each force component was within $\pm 4.11\%$. The measurement standard error for each component of force was found within $\pm 3.06\%$.

Surface roughness and sound level measurement

The machined workpiece's mean surface roughness was measured using a Mahrsurf PS 10 device. Before applying it for roughness measurement, it was calibrated using known sample roughness. The calibration standard error was found to be within $\pm 1.5\%$. The evaluation length was set to 4 mm while a cutoff of 0.8 mm. Three separate locations were utilized to take the surface roughness along the machined surface axis and the average measurement values were then calculated and presented as the final Ra. The whole noise produced by CNC machine and the cutting action during the machining is referred to as machining sound. The Lutron SL-401 sound meter, placed 1 m away from the machine to avoid any fluctuation, was used to record the machining sound. Before applying it for sound level measurement, it was calibrated using a known sound level. The calibration standard error was found to be within $\pm 1.3\%$. The experiments were executed three times, and the standard experimental mistakes for Ra and SL were estimated as $\pm 4.85\%$ and $\pm 3.23\%$, individually. The standard error was estimated as $\pm 2.04\%$ for Ra and $\pm 1.85\%$ for SL. The setups for measuring sound level and roughness are appeared in Fig. 3.

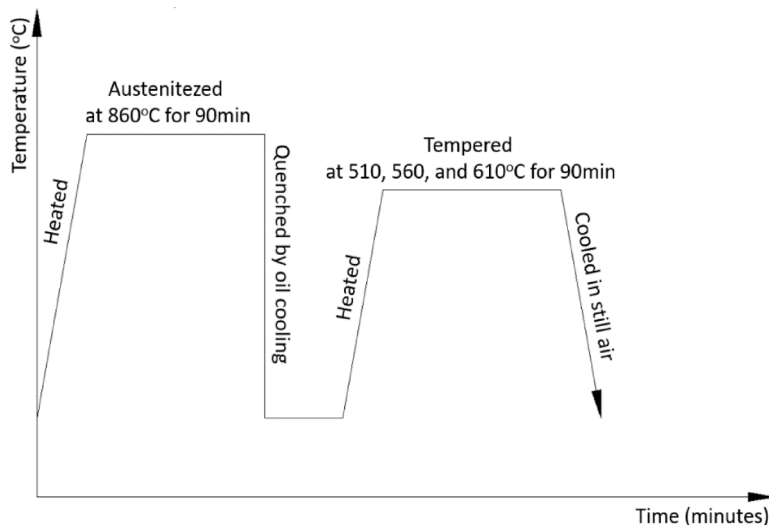


Fig. 1. The quenching and tempering heat cycle applied to AISI 4340 grade steel.





			
Cutting insert	Insert type-1	Insert type -2	Insert type -3
Brand	Kennametal	Kennametal	Walter
ISO code	CNMG 120408 CNMG 120408 CNMG 120408		
Chip breaker	MP	RP	NM4
Coatings	CVD (TiN-TiCN-TiN)	CVD (TiN-TiCN-TiN)	CVD (TiCN-Al ₂ O ₃ -TiN)
Tool holder			
	TCLNL 25 25 M12 (MRK)		
Tool holder geometry (mm)	25 × 25 × 150		
Length of cutting edge (mm)	12.896		
Thickness (mm)	4.763		
Nose radius (mm)	0.8		
Inclination angle	-6°		
Rake angle	-6°		
Approach angle	95°		
Clearance angle	7°		
Included angles	80°		

Table 1. Insert types and geometries.

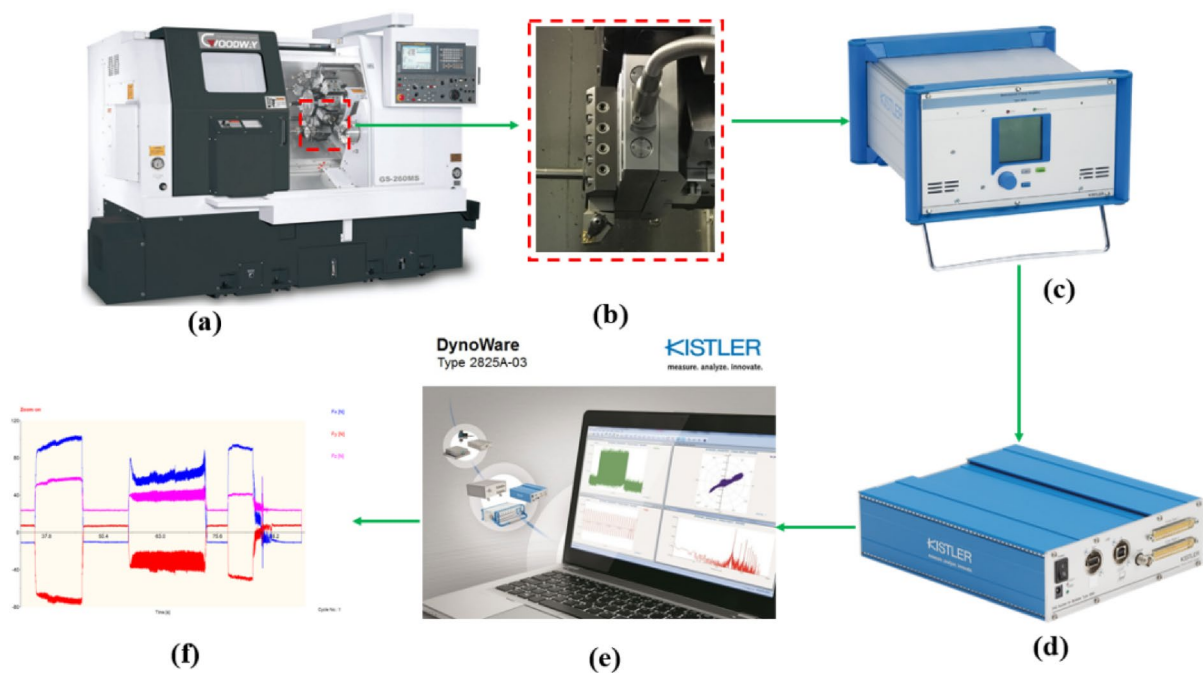


Fig. 2. Cutting force measurement arrangement in turning process: (a) CNC lathe, (b) dynamometer, (c) amplifier, (d) data acquisition, (e) dynoware software, (g) signal of forces.

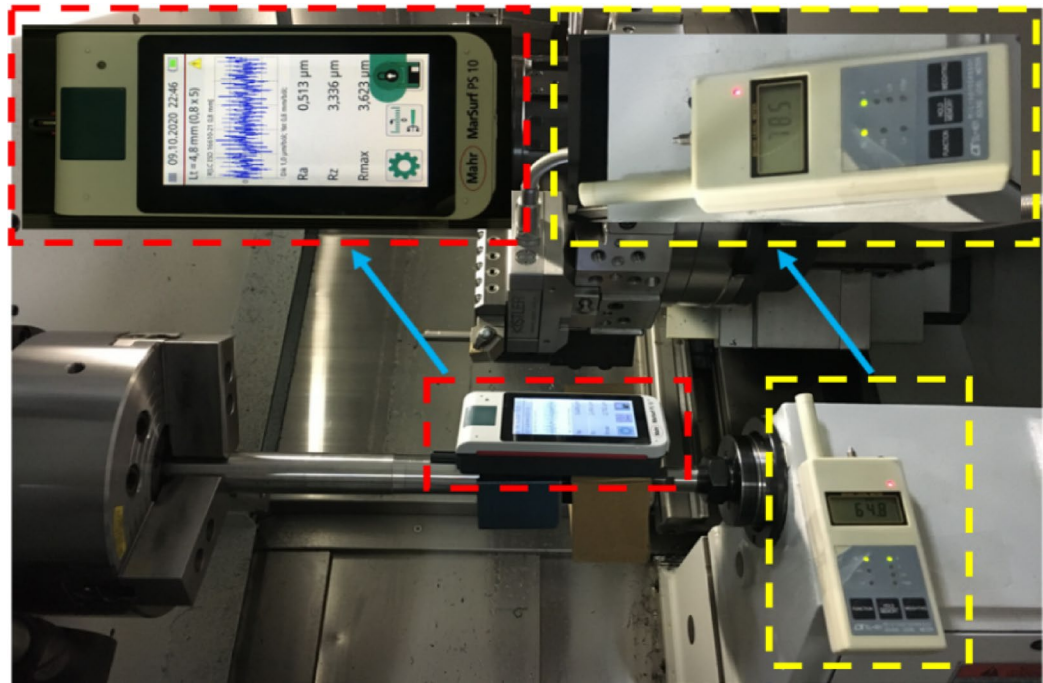


Fig. 3. Sound level and surface roughness measuring setup.

Power consumption measurement

The current value was measured using a digital multimeter (UNI-T UT 201). Before applying it to measure voltage, the multimeter was calibrated using known voltage. The calibration standard error was found to be within $\pm 1.2\%$. Total current measurement is provided by the instantaneous electrical current taken from the machine's electrical panel during the turning process. Firstly, instantaneous electric current was recorded for the machine running in cutting and non-cutting modes. Secondly, the current flowing through one phase of the servo motors in the CNC lathe was measured by the clamp amperemeter and then multiplied by three to find out the full current. Finally, the power consumption (P_c) was calculated using Eq. (1)^{69,70}.

$$P_c = \sqrt{3} * Volt. * I * Cos\theta \quad (1)$$

where (Volt. = 380) is voltage, (I) is current, and (Cos θ) is power factor, which is considered as 0.84 for the CNC lathe⁶⁹. The experiments were executed three times, and the standard error (experimental) for power consumption was estimated at $\pm 6.41\%$. The measurement standard error for power consumption was $\pm 2.34\%$.

Experimental procedure

The longitudinal dry hard turning process was accomplished on the AISI 4340 steel with a Goodway GS-260Y model 5-axis CNC lathe having a 15 kW motor power and a 4000 rpm max spindle speed. Taguchi L_9 orthogonal design (four factors and three levels) was used for the experimental testing. The input criteria studied include workpiece hardness (30, 35, 40 HRC), depth of cut (0.2, 0.3, 0.4 mm), cutting speed (175, 205, 235 m/min), and feed rate (0.10, 0.15, 0.20 mm/rev). The experimental setting was chosen grounded on the findings of Kechagias et al.⁷¹; they used L_{27} and L_9 designs for turning Titanium-alloys and recommended that the L_9 design was sufficient for studying machinability issues. Numerous other scientists have also adopted the L_9 design in machining studies^{72,73}. Each test had a cutting length of 20 mm, and a fresh cutting edge was utilized for every test to minimize the impact of tool wear. The performance-indicating responses like resultant force (F_r), surface roughness (Ra), power consumption (P_c), and machining sound (SL) are studied. Surface roughness was measured after each turning cycle, while sound level, current, and cutting forces were measured during the turning process. To minimize the experimental error during machining, each experiment was repeated three times, and the average data are mentioned in results and discussion section.

TOPSIS-sine cosine algorithm hybrid optimization

In this hybrid optimization process, TOPSIS is utilized to convert multi-response into a single response. Further, taking single response data, linear regression modeling was applied to develop a fitness function used in the sine-cosine algorithm to estimate the optimal solution. The steps of this hybrid optimization are shown in Fig. 4.

The details of the entire hybrid optimization process were discussed as follows:

TOPSIS is a popular method among multi-criteria decision-making methods^{74–76}. The TOPSIS method involves the following steps^{77,78}: First, a decision matrix using response data is created. In this matrix, rows

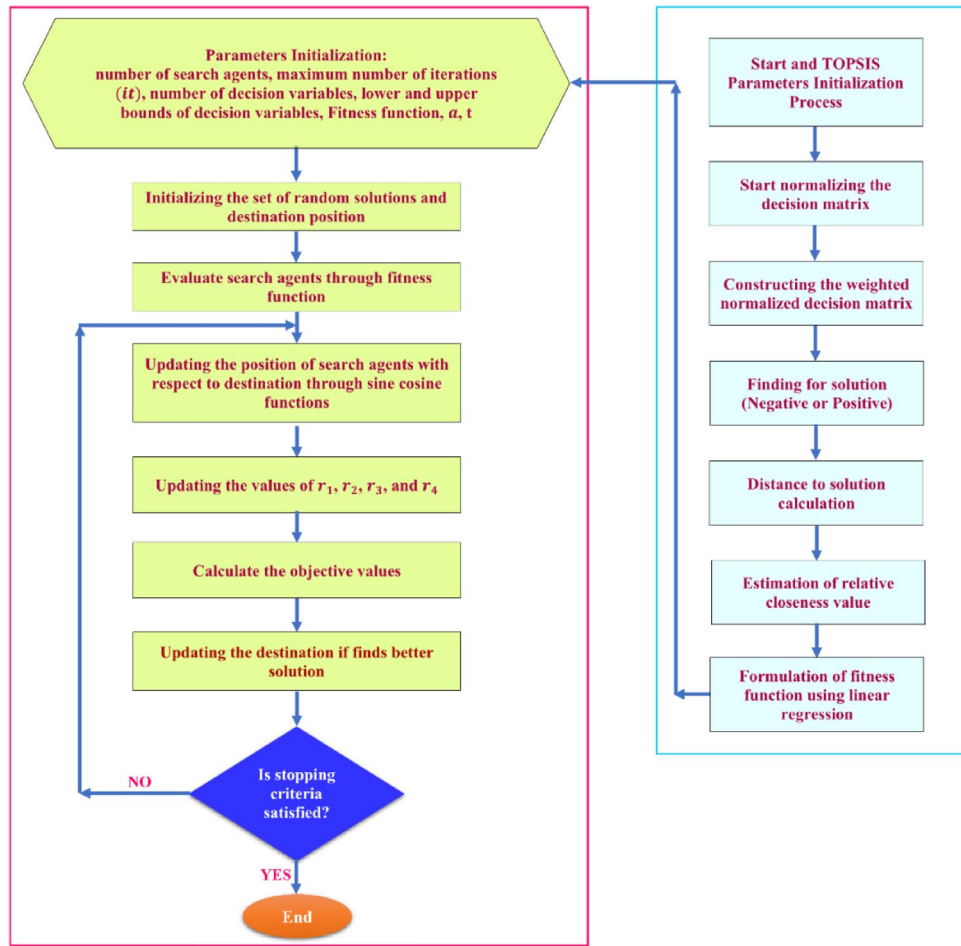


Fig. 4. Flow chart of TOPSIS-Sine Cosine Algorithm hybrid optimization.

represent criteria, while the columns correspond to evaluation factors⁷⁹. The second step is normalizing the decision matrix using Eq. (2).

$$V_x = \frac{N_{ij}}{\sqrt{\sum_{i=1}^n (N_{ij})^2}} \tag{2}$$

Here, $i = 1, 2, \dots, n, j = 1, 2, \dots, n, N_{ij}$ represents the real values of the i^{th} value of the j^{th} trial run, and V_x is the normalized data.

The third step involves constructing the weighted normalized decision matrix. Each element of the normalized decision matrix (V_x) is multiplied by the corresponding criterion weights (w_j), as shown in Eq. (3). This paper assigned an equal weight (0.25) to each response.

$$V_{ij} = V_x * w_j \tag{3}$$

In the fourth step, positive and negative ideal results are obtained. The best positive value (V_i^+) and the worst negative value (V_j^-) are determined by selecting the suitable value according to the relevant criteria using Eqs. (4) and (5), respectively.

$$V_i^+ = V_1^+, V_2^+, \dots, V_n^+ \tag{4}$$

$$V_j^- = V_1^-, V_2^-, \dots, V_n^- \tag{5}$$

where, $V_n^+ = \max V_{in}$, if n is a benefit attribute, $= \min V_{in}$, if n is a cost attribute.

$V_n^- = \min V_{in}$, if n is a benefit attribute, $= \max V_{in}$, if n is a cost attribute⁷⁶

At this stage, the distance values from the ideal solution are determined. The deviations of the alternatives from the positive and negative ideal results are obtained by the Euclidean distance. These deviation values are referred to as the “ideal best values (S_i^+)” and ideal worst values (S_i^-), which can be computed using Eqs. (6) and (7), respectively.

$$S_i^+ = \sqrt{\sum_{j=1}^m (V_{ij} - V_j^+)^2} \quad (6)$$

$$S_i^- = \sqrt{\sum_{j=1}^m (V_{ij} - V_j^-)^2} \quad (7)$$

The fifth step involves determining the relative closeness value (P_i) to the ideal solution. This is obtained by using the positive and negative ideal separations, where the negative ideal separation measure is divided by the total ideal separation measure. The calculation is performed using Eq. (8).

$$P_i = \frac{S_i^-}{S_i^- + S_i^+}, 0 \leq P_i \leq 1 \quad (8)$$

After calculating the relative closeness value for all the alternatives, the fitness function for each insert type was developed using linear regression modeling. The fitness functions for the algorithm are developed through Minitab 17 software, and the generalized Equation for the fitness function is displayed using Eqs. (9), where P_i is the measured response and is used in an SCA algorithm as a fitness function, C , C_1 , C_2 , C_3 , and C_4 are constants, and H , V , f , and a are input variables.

$$P_i = C + (C_1 * H) + (C_2 * V) + (C_3 * f) + (C_4 * a) \quad (9)$$

In the next step, the Sine Cosine Algorithm (SCA) was used to find optimal or near-optimum values of different machining parameters in this paper. SCA is a population-grounded optimization algorithm that uses the sine and cosine trigonometric functions to solve optimization problems⁶². Figure 5 shows the basic flowchart of SCA, which reveals the algorithm's essential steps. In SCA, the solutions to the given problems can be updated through Eqs. (10) and (11).

$$X_i^{t+1} = X_i^t + x_1 \cdot \sin(x_2) \cdot |x_3 m_i^t - X_i^t| \quad (10)$$

$$X_i^{t+1} = X_i^t + x_1 \cdot \cos(x_2) \cdot |x_3 m_i^t - X_i^t| \quad (11)$$

where, X_i^t shows the position of the current solution of a problem in i^{th} dimension at t^{th} iteration, x_1 , x_2 , and x_3 define the random numbers, m_i reveals the target point position in i^{th} dimension. The term $||$ is used to get the absolute value.

The equations mentioned above are combined by considering Eq. (13).

$$X_i^{t+1} = \begin{cases} X_i^t + x_1 \cdot \cos(x_2) \cdot |x_3 m_i^t - X_i^t|, & \text{if } x_4 < 0.5 \\ X_i^t + x_1 \cdot \sin(x_2) \cdot |x_3 m_i^t - X_i^t|, & \text{if } x_4 \geq 0.5 \end{cases} \quad (12)$$

where, x_4 gives a random number vector and lies between $[0 \ 1]$ in the algorithm.

The above equations have four important parameters: x_1 , x_2 , x_3 , and x_4 . The parameter x_1 defines the movement direction in a search space or region. Similarly, the parameter x_2 indicates the direction of movement, whether towards or away from the destination. The third parameter x_3 offers the random weights to the destination m_i . The last parameter x_4 is a random number vector and remains between $[0 \ 1]$ in the algorithm.

Results and discussion

The present study examines the influence of various input variables (hardness: H , feed rate: f , cutting speed: V , depth of cut: a) and three inserts on the (Fr), (Ra), (SL), and (Pc). The test results are displayed in Table 2.

Assessment of resultant force

To estimate the resultant force, the (F_x), (F_y), and (F_z) forces are recorded with a Kistler dynamometer. The force signals obtained in the first three runs for each insert type are depicted in Fig. 5a–c. Further, the (Fr) was calculated using the force resultant formula, and values are displayed in Table 2. The comparison of resultant force between the three inserts is depicted in Fig. 5d. The bar charts (Fig. 5d) affirmed that insert type-3 produced better results (lower cutting forces) than other inserts. Insert type-2 produced the most significant resultant forces among them. Taking the average of all 9 data, insert type-1 produced 8.67% higher resultant force than insert type-3, while insert type-2 produced 36.69% greater resultant force than insert type-3.

Similarly, insert type-2 produced a 25.78% greater resultant force than insert type-1. Based on this estimation, it can be said that the insert type-3 was best among these three inserts. Also, the intermediate layer Al_2O_3 may work better than the other tool coating layer, as its thermal conductivity was reduced with increasing temperature, thus working as a protective layer for the bottom layer as well as the substrate⁸⁰. Awadh et al.⁴⁵ also performed medium hard turning research on AISI 4340 steel using CVD, and PVD inserts and found better results than the current research. TiAlSiN coated tool outperformed among all types of inserts. The maximum resultant force was

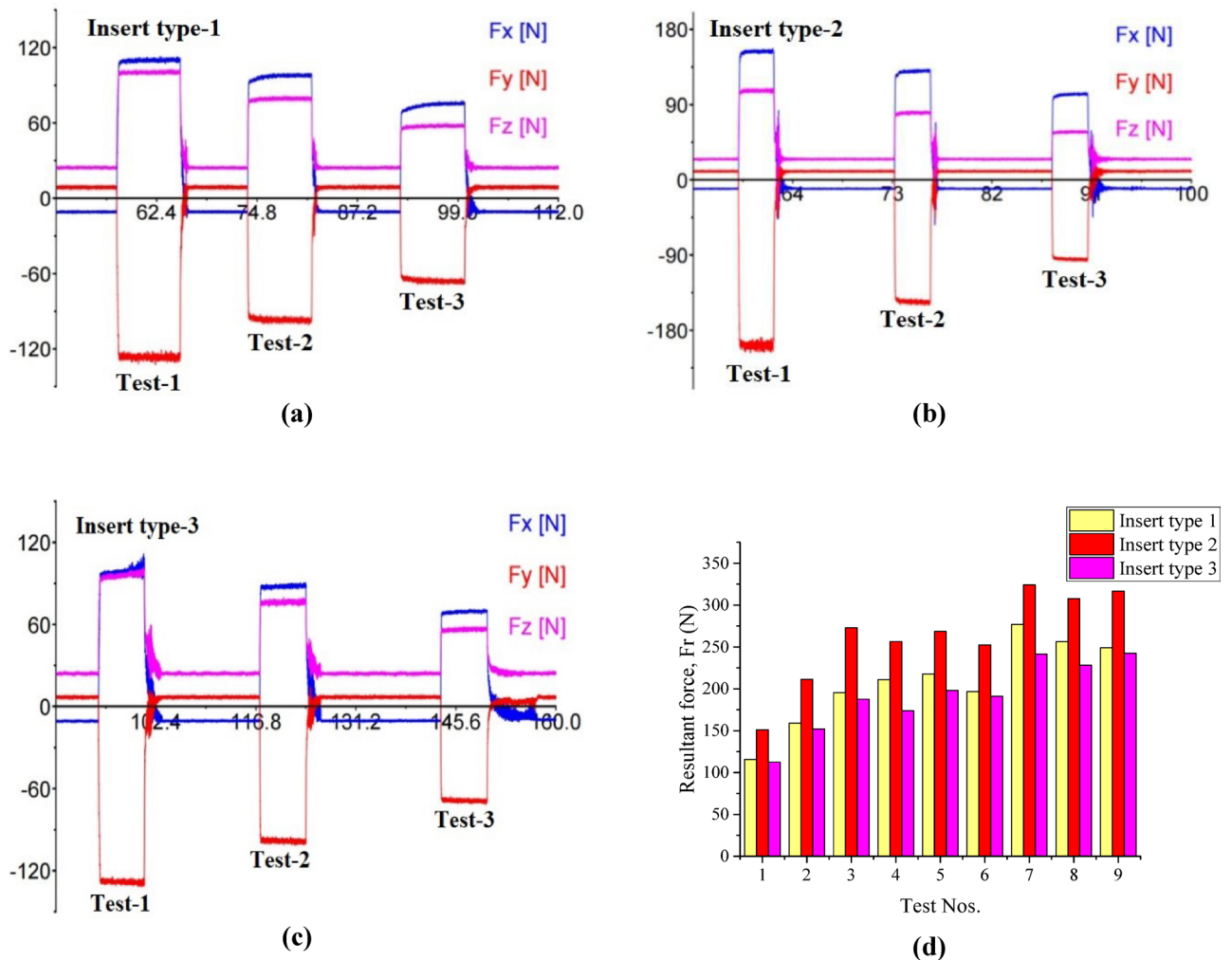


Fig. 5. (a–c) Force signals obtained for test-1, test-2, and test-3 (d) Comparisons of resultant force obtained for three different types of cutting inserts.

found as 66.22 N which is 266% lower than the current resultant force of type 3 insert. Although, the previous research is good for machinability point of view but the tooling cost is higher.

Surface and main effects plots were used to show the impact of the input factors on the resultant force. For each type of insert, the hardness of the workpiece played an essential role as the resultant force was almost linearly elevated with the leading hardness of the workpiece (Fig. 6a–c). Bouacha et al.⁸¹ found that all three cutting forces increased with leading hardness and rising speed (greater than 130 m/min) in the turning of hardened bearing steel. These results show that power usage increased as cutting speed changed from 175 to 235 m/min, and work hardness ranged from 30 to 40 HRC. The second important input was the feed rate for each type of insert. For insert type-1, the cutting speed was traced to be least important, while for the other two inserts, the depth of cut was identified as least important. Except for insert type-1, the higher resultant force was found when the feed and cutting speeds were higher. Demirpolat et al.⁸² accomplished machining trials on hardened bearing steel and discovered that the highest cutting force could be achieved with an elevated machining speed and tool feed in a dry condition. Similarly, the turning forces were most influenced by the depth of cutting, followed by tool feed, in machining 4340 steel⁵².

Moreover, surface plots (Fig. 6d–f) for each insert type were plotted using hardness and cutting speed parameters. The resultant force was gained for each type of insert with a simultaneous increase in turning speed and hardness. The highest resultant force was achieved when machining was done on the highest hardness test piece (40-HRC) with the maximum speed (235 m/min), while the smallest resultant force was seen on the minimum hardness test piece (30-HRC) with the least cutting speed (175 m/min). In each plot, the curve was lifted at the middle portion, ensuring the gain in resultant force at medium test piece hardness and speed levels. Overall, it can be concluded that the hardness of the workpiece is the most important index for hard turning concerns, followed by feed rate. Thangarasu et al.⁸³ discovered that the collective effect of two factors (feed-cutting depth) on cutting force is greater (50.4%) than the individual effects of feed and cutting depth.

Test no	Insert type	Input variables				Responses investigated			
		<i>H</i> (HRC)	<i>V</i> (m/min)	<i>f</i> (mm/rev)	<i>a</i> (mm)	<i>Fr</i> (N)	<i>Ra</i> (μm)	<i>SL</i> (dB)	<i>Pc</i> (W)
1	1	30	175	0.10	0.2	115.71	0.330	77.67	3591
2	1	30	205	0.15	0.3	158.87	0.436	79.84	3744
3	1	30	235	0.20	0.4	195.36	0.566	81.65	3897
4	1	35	175	0.15	0.4	210.90	0.831	81.43	4132
5	1	35	205	0.20	0.2	217.60	0.977	82.32	4098
6	1	35	235	0.10	0.3	196.80	0.712	83.08	4103
7	1	40	175	0.20	0.3	276.80	1.460	83.78	4488
8	1	40	205	0.10	0.4	256.23	1.165	84.19	4454
9	1	40	235	0.15	0.2	248.96	1.371	84.56	4404
10	2	30	175	0.10	0.2	151.16	0.457	79.46	3541
11	2	30	205	0.15	0.3	211.35	0.537	80.09	3741
12	2	30	235	0.20	0.4	272.87	0.618	80.73	3942
13	2	35	175	0.15	0.4	256.50	0.952	82.78	4123
14	2	35	205	0.20	0.2	268.54	1.026	83.65	4167
15	2	35	235	0.10	0.3	252.45	0.824	82.48	4120
16	2	40	175	0.20	0.3	324.22	1.546	84.87	4395
17	2	40	205	0.10	0.4	307.64	1.243	84.15	4338
18	2	40	235	0.15	0.2	316.52	1.322	84.98	4399
19	3	30	175	0.10	0.2	112.44	0.312	77.32	3508
20	3	30	205	0.15	0.3	152.06	0.408	78.23	3673
21	3	30	235	0.20	0.4	187.57	0.522	79.05	3836
22	3	35	175	0.15	0.4	173.80	0.787	81.00	3994
23	3	35	205	0.20	0.2	198.11	0.812	80.61	4012
24	3	35	235	0.10	0.3	191.20	0.634	81.32	4105
25	3	40	175	0.20	0.3	241.51	1.238	83.37	4321
26	3	40	205	0.10	0.4	228.17	0.986	83.25	4303
27	3	40	235	0.15	0.2	242.54	1.027	83.12	4308

Table 2. Input and response variables for the experimental study.

Assessment of surface roughness

The most important metric for evaluating the surface quality in the finish-machining process is surface roughness (*Ra*). The cutting inserts have a significant impact on surface quality. Therefore, the current research uses three different inserts to investigate the surface quality obtained by turning three different hardness levels of the workpiece. Insert type-3 gave better results (lower *Ra*) than the other two inserts among the three different inserts. Insert type-2 corresponds to larger roughness in comparison to other type inserts. The most considerable *Ra* value of 1.546 μm was received when turning a 40 HRC workpiece using insert type-2 and the lowest speed (175 m/min), highest feed (0.2 mm/rev), and moderate depth of cut (0.3 mm). The lowest *Ra* was achieved as 0.312 μm when the experiment was accomplished on the minimum workpiece hardness (30 HRC) with the lowest levels of input parameters. By taking the mean result of 9 data, the *Ra* for insert type-1 is 0.872 μm, for insert type-2 is 0.947 μm, and insert type-3 is 0.747 μm. Therefore, insert type-1 produced 16.68% greater *Ra* than insert type-3, while insert type-2 produced 26.74% greater *Ra* than insert type-3. Similarly, insert type-2 produced 8.62% greater *Ra* than insert type-1. The obtained results are similar to the previous study results considering the hard turning of AISI 4340 steel^{84,85}. Al Awadh et al.⁴⁵ found the superior performance of second-generation PVD-coated TiAlSiN carbide tools over CVD and PVD-applied tools. The minimum *Ra* was found as 0.19 μm, lower than the minimum *Ra* obtained in the current research. Besides, they found maximum *Ra* of 0.74 μm, while in the current study the maximum *Ra* was found as 1.546 μm.

Furthermore, surface plots and main effects graphs were used to show how input variables affected surface roughness. By analyzing and comparing the main effects graphs (Fig. 7a-c) for each type of insert, *Ra* was impacted mainly by the test piece hardness, which rose rapidly with the leading hardness. The feed had the second largest impression on the *Ra*, which was leading with an increasing feed. A rise in roughness was also documented by Bhuiyan and Choudhury⁸⁶ with growing workpiece hardness. Ozel et al.⁸⁷ showed a slight rise in *Ra* during the hard machining of AISI H11 steel as the workpiece hardness intensified from 51 to 55 HRC.

Additionally, *Ra* was also expressively prejudiced by the feed rate. In another work⁸⁸, it was reported that the workpiece hardness, cutting depth, and tool feed had relevant stimuli on *Ra*. The term cutting speed has an insignificant impact on *Ra* for insert type-1, while for other types of inserts, a marginal reduction in *Ra* was found when the speed was rising. Similarly, the cutting depth had a minor consequence on *Ra*. Surface plots (Fig. 7d-f) showed the rising slope of the graph in a diagonal direction; thus, it can be said that with the gain in workpiece hardness and feed, the surface roughness was raised. The largest *Ra* was achieved when the workpiece hardness and feed were maximum.

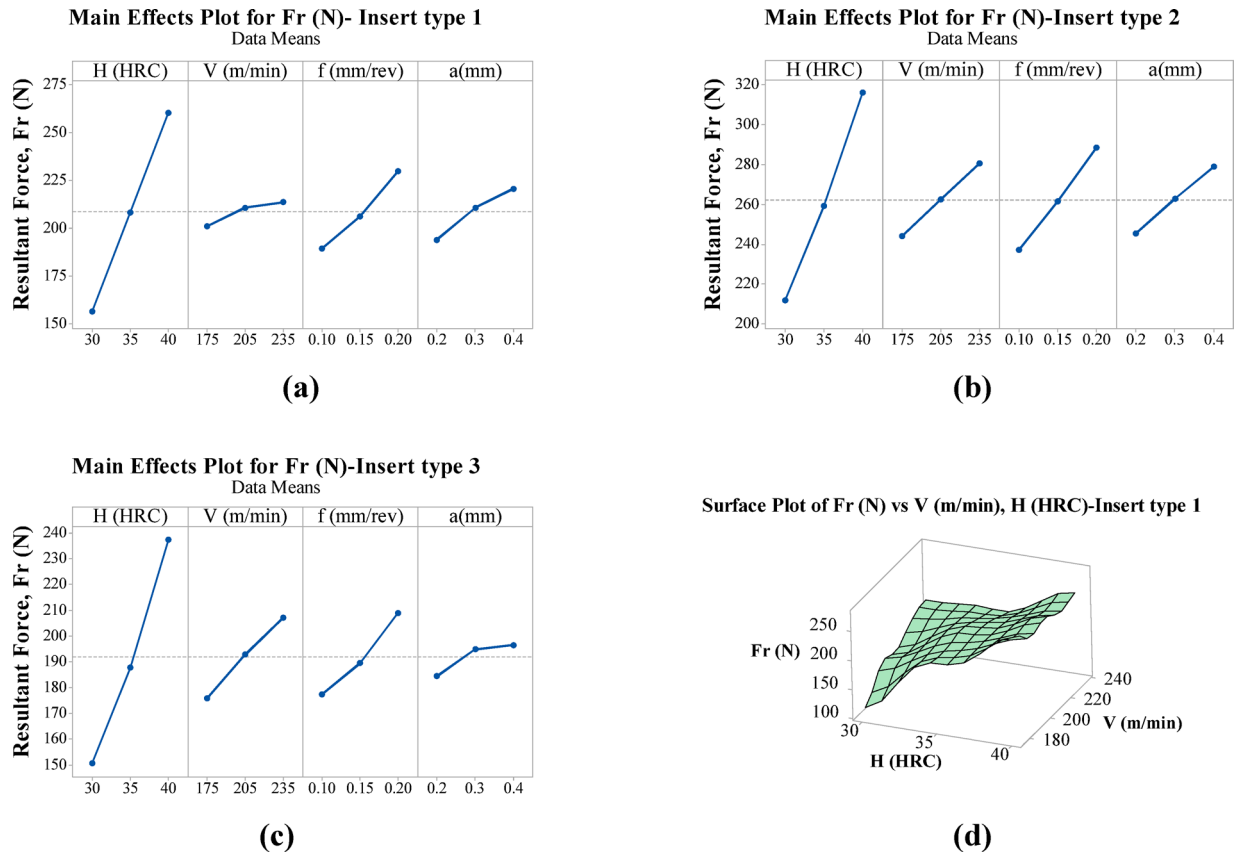


Fig. 6. Graphical plots for resultant force-Fr (a–c) main effects plot (d–f) surface plots.

Assessment of sound level

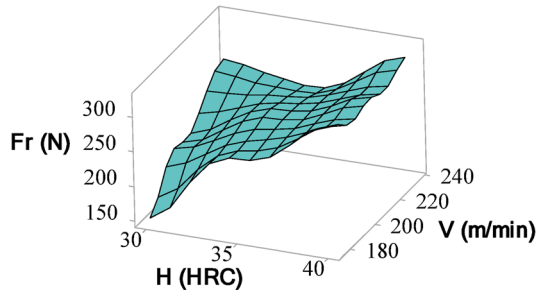
Almost all machine shops have sound emissions, which frequently exceed the level of health hazards. The noise level from cutting operations puts operators and people working in the same area at risk for health issues. The Occupational Health and Safety directive states that all precautions for sound creation in workplaces should be removed or minimized at the source⁸⁹. Commonly, two sound sources are produced during dry hard turning: the CNC lathe when it is operating and the cutting action caused by the dynamic interaction of two hard materials (hardened steel and carbide insert). Therefore, it is impossible to eliminate sound generation, but it can be reduced by choosing a stiffer CNC lathe and choosing the right amount of cutting parameters. Besides, cutting parameters levels, hardness of the workpiece, cutting tool materials, and geometry greatly affected the sound level. Therefore, it is crucial to choose the optimum parameters correctly to reduce the sound level during heavy machining^{90–92}. Considering these factors, the current study analyses the sound level when three different hardened steel workpieces are machined using three distinct cutting inserts.

Based on the experimental observations (Table 2), the maximum sound level for inserts type 1, type 2, and type 3 are found as 84.56 dB, 84.98 dB, and 83.37 dB, while the minimum sound level for inserts type 1, type 2 and type 3 are found as 77.67 dB, 79.46 dB, and 77.32 dB. However, the machining with insert type-2 produced the highest sound level compared to other inserts. Similarly, the lowest sound level was created with insert type-3. Awadh et al.⁴⁵ found the minimum and maximum noise level 79.1 dB, and 89.0 dB, respectively in turning AISI 4340 steel using PVD and CVD inserts. In compare to previous study, the current research showed less noise emission.

The sound level evolved during current machining research was less than 85 dB. According to the National Institute on Deafness and Other Communication Disorders, prolonged or repeated exposure to noise of 85 dB or above can lead to hearing loss⁹³. Therefore, the sound level results for all distinct types of inserts are safe but still require a lower sound level for a better environment and social sustainability. Therefore, identifying the consequences of input factors on cutting sound level is essential.

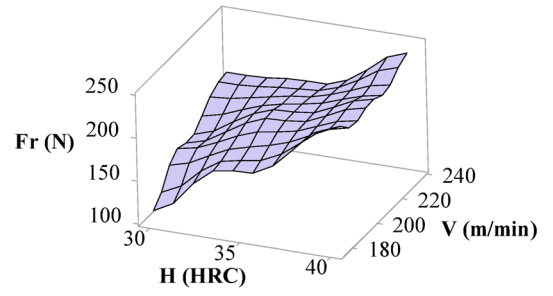
The consequence of input variables on sound level was depicted with main effects plots and surface plots. For each type of insert, the workpiece hardness had the most significant stimulus on the sound level as the graph line sharply increased when the test specimen hardness rose from 30 to 40 HRC (Fig. 8a–c). The test specimen hardness also has a substantial impact on the cutting forces. For insert type-1, the second largest impact term towards sound level was cutting speed, while for insert type-2 and insert type-3, it was feed and cutting depth, respectively. Moreover, the sound level rose with the growth in all input terms except for insert type-2; the cutting depth had a minor impression as the graph line lay near the mean line (constant value). Al Awadh et al.⁴⁵ discovered that the sound in cutting quickly increased with growing speed because of the greater vibration due

Surface Plot of Fr (N) vs V (m/min), H (HRC)-Insert type 2



(e)

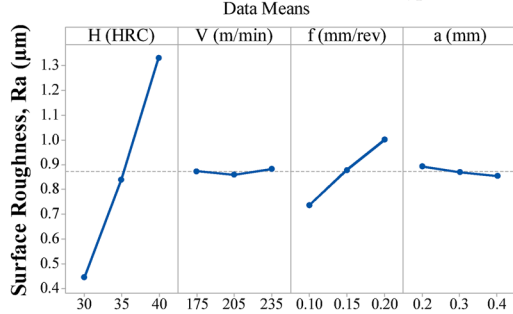
Surface Plot of Fr (N) vs V (m/min), H (HRC)-Insert type 3



(f)

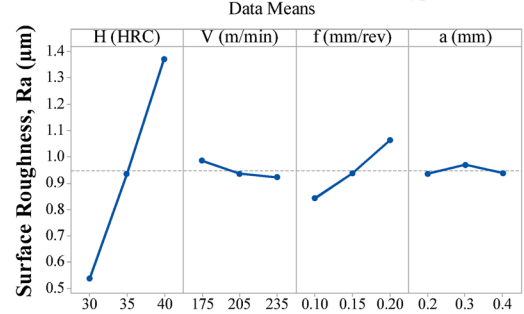
Fig. 6. (continued)

Main Effects Plot for Ra (μm) - Insert type 1



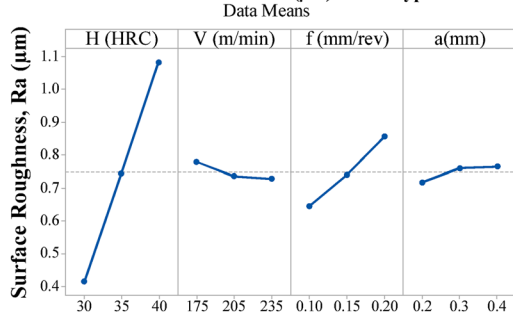
(a)

Main Effects Plot for Ra (μm) - Insert type 2



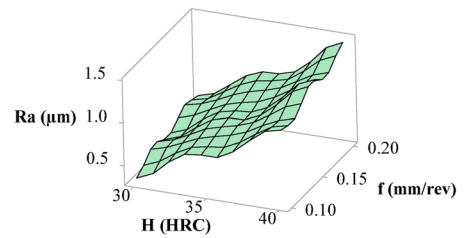
(b)

Main Effects Plot for Ra (μm) - Insert type 3



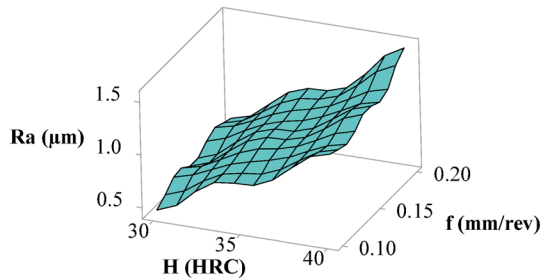
(c)

Surface Plot of Ra (μm) vs f (mm/rev), H (HRC)- Insert type 1



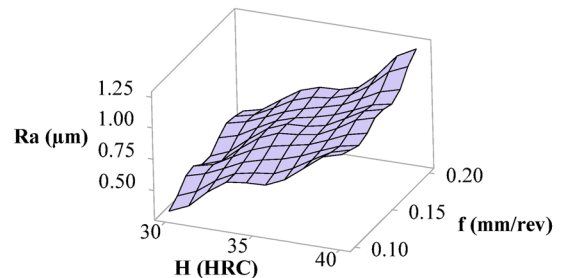
(d)

Surface Plot of Ra (μm) vs f (mm/rev), H (HRC)- Insert type 2



(e)

Surface Plot of Ra (μm) vs f (mm/rev), H (HRC)- Insert type 3



(f)

Fig. 7. (a–c) Main effects plot and (d–f) surface plots for surface roughness.

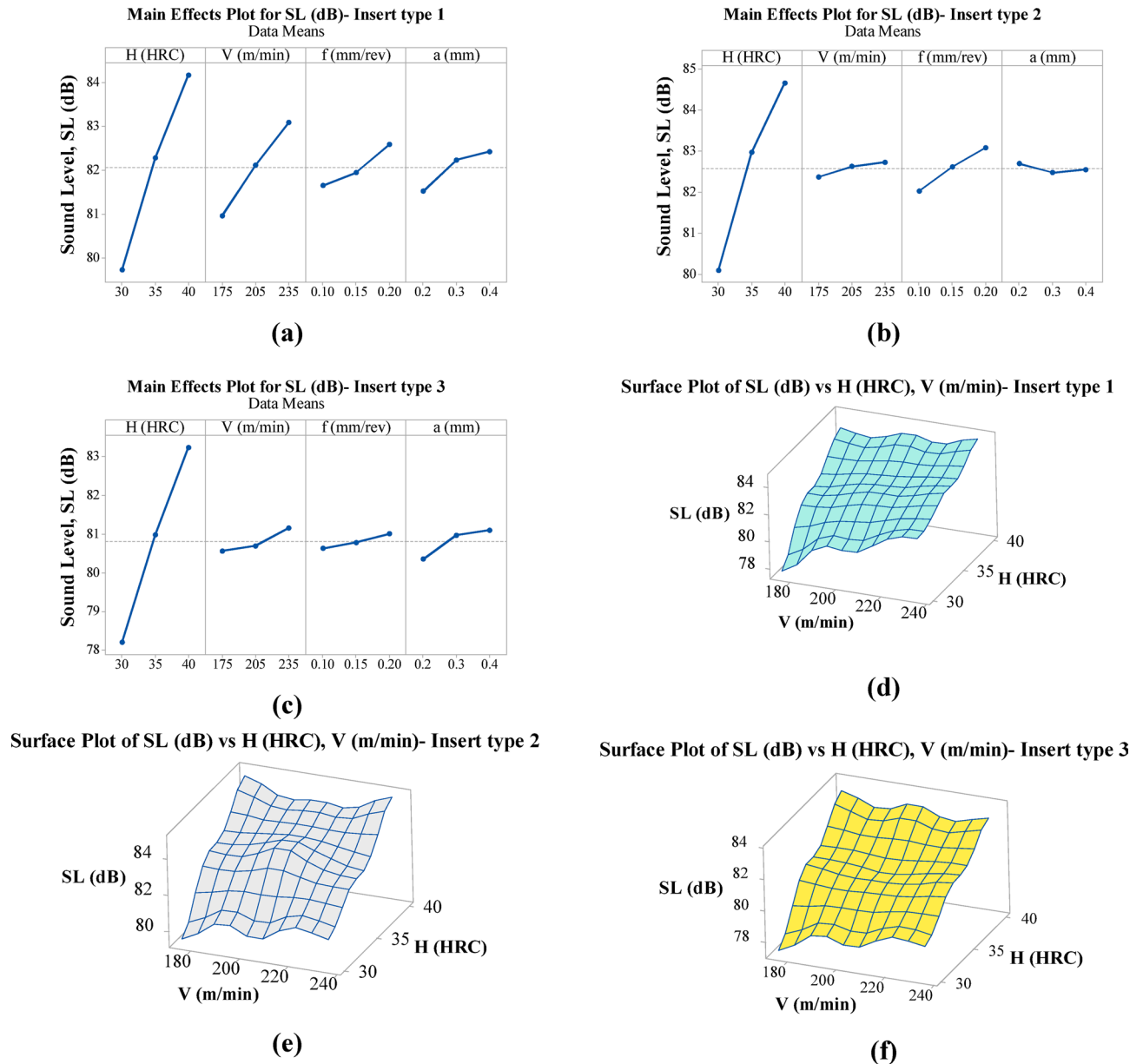


Fig. 8. (a–c) Main effects plot and (d–f) surface plots for sound level.

to the larger speed turning of AISI 4340 grade steel. Several researchers also agreed that the cutting speed had an enormous impact on cutting sound development during machining^{91–93}.

Similarly, for each insert type, the surface slope was diagonally increasing with simultaneous increments in cutting speed and workpiece hardness (Fig. 8d–f). The surface plot was lifting marginally in the middle due to the leading sound level at middle levels of speed and workpiece hardness. For each type of insert, the lowest sound level was achieved when cutting speed and hardness had the lowest values. Similarly, when the machining was executed at the maximum level of speed and workpiece hardness, the sound level was highest for the insert type-1, whereas, for other inserts, the most significant sound level was noticed at a lower speed with the highest hardness workpiece.

Assessment of power consumption

Power consumption is one of the main critical parameters that affect the overall machining cost. The input process parameters and cutting circumstances substantially impact power utilization⁹⁴. Determining optimal input variables and cutting conditions is essential for designing machine tools that consume lesser energy overall. This research used three distinct coated steel inserts to evaluate the power consumption in machining three different hardness levels of the AISI 4340 steel workpiece. The maximum power consumption for insert types 1, 2, and 3 is found as 4488 W (Run 7), 4399 W (Run 18), and 4321 W (Run 25). In comparison to this study, Awadh et al.⁴⁵ found 4065 W maximum power consumption using TiAlSiN coated insert, which was lower

than the current findings. Similarly, minimum power consumption for insert types 1, 2, and 3 are found as 3591 W (Run 1), 3541 W (Run 10), and 3508 W (Run 19). In comparison to this results, Awadh et al.⁴⁵ found 2985 W minimum power consumption, showing better performance than the current study. The minimal power consumption for each tool was recorded at the lowest level of input factor ($a=0.10$ mm, $f=0.10$ mm/rev, $H=30$ HRC, and $v=175$ m/min). It might be possible because of the lesser force required to remove the minimum workpiece hardness at the first levels of input variables. Considering an average of 9 test results for each insert, the power consumption using insert type-1 is 2.36% higher than insert type 3, while power consumption using insert type-2 is 1.95% greater than insert type-3. Similarly, the power consumption using insert type-1 and type-2 is very close (insert type-1 has 0.39% higher power consumption than type-2). Overall, insert type-3 is best for less power consumption among all inserts considered. Therefore, insert type-3 is recommended for mass production. Al Awadh et al.⁴⁵ testified that the TiAlSiN-coating tool produced the least turning force when machining AISI 4340 hardened grade steel compared to the TiAlN and TiN-coated carbide tools, resulting in decreased power expenditure.

Moreover, the impact of the process variables and workpiece hardness on power consumption was illustrated with main effects plots (Fig. 9a-c) and surface plots (Fig. 9d-f). Power consumption increased significantly for each insert as workpiece hardness improved (Fig. 9a-c). It was also raised with the leading process variables. According to Nur et al.⁹⁵, a workpiece turning at greater speeds requires more power since the motor needs more energy to run at such speeds. Additionally, it was also implied that power consumption was greatly affected by feed and speed during dry cutting. The current result data (Table 2) shows that the resultant force was rising

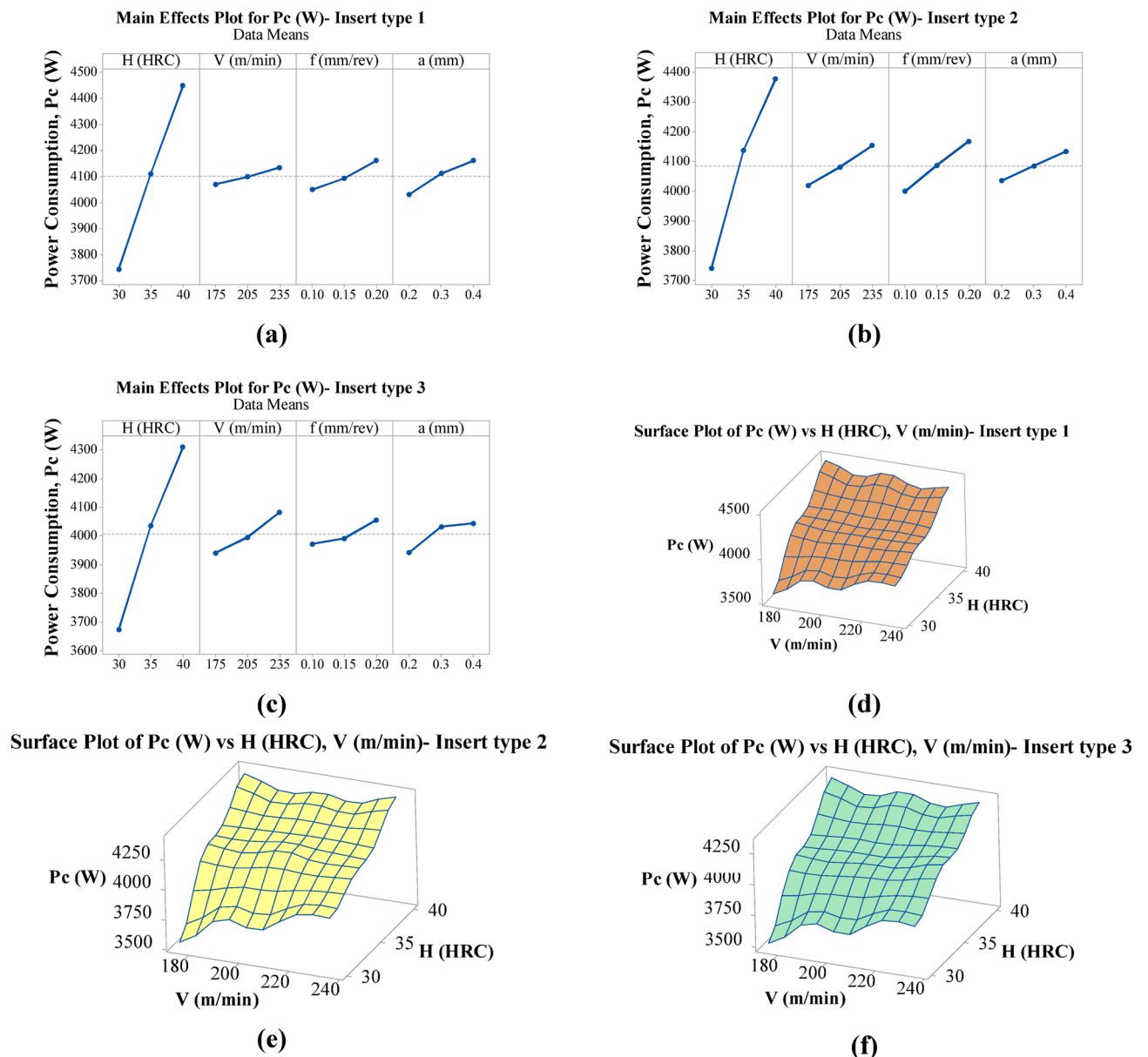


Fig. 9. (a–c) Main effects plot and (d–f) surface plots for power consumption.

	Fr	Ra	SL	P
Insert Type-1				
V ⁺	0.10786	0.02892	0.07885	0.07277
V ⁻	0.04509	0.12793	0.08585	0.09095
Insert Type-2				
V ⁺	0.10104	0.03767	0.08017	0.07207
V ⁻	0.04711	0.12743	0.08573	0.08953
Insert Type-3				
V ⁺	0.10306	0.03245	0.07971	0.07279
V ⁻	0.04778	0.12877	0.08595	0.08966

Table 3. Results of the best positive value (V⁺) and the worst negative value (V⁻).

Run	Insert Type-1			Insert Type-2			Insert Type-3		
Nos	S _i ⁺	S _i ⁻	Pi	S _i ⁺	S _i ⁻	Pi	S _i ⁺	S _i ⁻	Pi
1	0.06277	0.10091	0.61651	0.05393	0.09161	0.62944	0.05528	0.09798	0.63931
2	0.04703	0.09265	0.66327	0.03602	0.08643	0.70584	0.03987	0.08913	0.69090
3	0.03859	0.08516	0.68813	0.02237	0.08598	0.79355	0.03274	0.08177	0.71406
4	0.05216	0.06690	0.56187	0.04755	0.05925	0.55476	0.05839	0.05415	0.48113
5	0.06224	0.05861	0.48497	0.05177	0.05656	0.52208	0.05641	0.05777	0.50596
6	0.04722	0.07319	0.60784	0.03953	0.06764	0.63111	0.04204	0.07135	0.62921
7	0.10086	0.06277	0.38363	0.09158	0.05393	0.37061	0.09798	0.05484	0.35885
8	0.07594	0.06055	0.44363	0.06715	0.05480	0.44939	0.07253	0.05572	0.43445
9	0.09358	0.05253	0.35951	0.07365	0.05473	0.42634	0.07643	0.05947	0.43761

Table 4. Calculated results of the ideal best (S_i⁺), ideal worst (S_i⁻), and relative closeness value (Pi).

with increasing speed and tool feed rate, impacting the increase in power usage. This outcome is consistent with an empirical test on the cutting of AISI 1045 steel, which found that the power consumption constantly rises as the cutting speed increases⁹⁶. Moreover, surface plots for each insert type (Fig. 9d-f) ensured the leading power consumption with leading hardness and cutting speed.

Optimization results

The step-wise results for TOPSIS-Sine cosine algorithm hybrid optimization are discussed as follows:

In the first step, the decision matrix using response data is created (Table 2). The response results (Table 2) of runs 1–9, runs 10–18, and runs 19–27 are the decision matrix for Insert type-1, type-2, and type-3, respectively. In the second step, normalized data was evaluated using Eq. 2. In the third step, the weighted normalized matrix was estimated from Eq. 3.

In the 4th step, the best positive value (V⁺) and the worst negative value (V⁻) are estimated using Eqs. (4) and (5), respectively, and the results are displayed in Table 3. At this stage, “The ideal best values (S_i⁺)” and the ideal worst values (S_i⁻)” are also estimated using Eqs. (6) and (7), respectively, and the values are mentioned in Table 4. In the 5th step, Eq. 8 was used to estimate the relative closeness value to the ideal solution, and the estimated data are mentioned in Table 4.

Now, the multi-response data was converted into a single response Pi. Further, the fitness function for each insert type was developed using the linear regression modeling concept (Eq. 9). The fitness functions for the algorithm are developed through Minitab 17 software and displayed using Eqs. (13), (14), and (15).

$$Pi (Insert - type - 1) = 1.279 - (0.02604 * H) + (0.000519 * V) - (0.371 * f) + (0.388 * a) \quad (13)$$

$$Pi (Insert - type - 2) = 1.1590 - (0.029416 * h) + (0.001646 * V) - (0.0790 * f) + (0.3664 * a) \quad (14)$$

$$Pi (Insert - type - 3) = 1.1876 - (0.02711 * h) + (0.001676 * V) - (0.414 * f) + (0.0779 * a) \quad (15)$$

In the next step, using the fitness function, the Sine Cosine Algorithm (SCA) was used to search optimal or near-optimum values of different machining parameters in this paper. The conceptual details are reported in “TOPSIS-sine cosine algorithm hybrid optimization” section. The values Pi were obtained after compiling the algorithm 2–3 times, with the condition of 1000 iterations. For insert type-1, the optimum or best fitness value Pi is obtained to be 0.62912 concerning the following local best fitness values of the inputs: a (mm)=0.2, f (mm/rev)=0.1, V (m/min)=175, and H(HRC)=30. Their corresponding global best fitness outputs are Fr=116.34 N, Ra=0.450 μm, SL=79.65 dB, and P=3566 W, respectively. Similarly, for insert type-2, the best fitness value of 0.62995 Pi concerning the following local best fitness input values: a (mm)=0.2, f (mm/rev)=0.1, V (m/

Aspect	Current research	Previous research ⁴⁵
Optimization methods	TOPSIS-Sine cosine algorithm	Grey-Crow Search algorithm
Best optimal cutting parameters and responses	$a = 0.2$ mm, $f = 0.1$ mm/rev, $V = 190$ m/min, and $H = 30$ HRC and their corresponding global best fitness outputs are $F_r = 118.80$ N, $R_a = 0.363$ μ m, $SL = 77.57$ dB, and $P = 3559$ W	$H = 32$ HRC, $V = 220$ m/min, $f = 0.04$ mm/rev, and $a = 0.0865$ mm, and their corresponding global optimum machine parameters of the output (dependent) variables are: $F_r = 47.05$ N, $R_a = 0.269$ μ m, $SL = 83.815$ dB, and $P = 3356$ W
MRR (Highest)	3800 mm ³ /min	761.2 mm ³ /min

Table 5. Comparative results.

min) = 180, and H (HRC) = 30, and their corresponding global best fitness outputs are $F_r = 152.46$ N, $R_a = 0.450$ μ m, $SL = 79.65$ dB, and $P = 3567$ W, respectively. Moreover, for insert type-3, the best fitness value is 0.67027 for P_i concerning the following local best fitness input values: $a = 0.2$ mm, $f = 0.1$ mm/rev, $V = 190$ m/min, and $H = 30$ HRC and their corresponding global best fitness outputs are $F_r = 118.80$ N, $R_a = 0.363$ μ m, $SL = 77.57$ dB, and $P = 3559$ W, respectively. The energy consumption at optimal conditions was estimated and compared with these three inserts. The energy consumption for insert type-1, type-2, and type-3 was estimated as 2.428 kJ, 2.361 kJ, and 2.235 kJ, respectively. Therefore, the insert type-3 consumed 7.95% lower energy than type-1 and 5.33% lower than type-2. Further, as a result of the optimal condition, the carbon emission was estimated using Eq. 16⁹⁷. The carbon emission was calculated as 0.0172 KgCO₂, 0.0167 KgCO₂, and 0.0158 KgCO₂ for insert type-1, type-2 and type-3, respectively. Therefore, insert type-3 produced 8.14% lower carbon emission in comparison to insert type-1 while 5.39% lower than Insert type-2. Furthermore, the current optimal results are compared with previous results as shown in Table 5. The optimum results from the previous study were better than current study, but metal removal rate in the current study was very high in comparison with the previous research.

$$C_E = \frac{P \times C_T \times C_{EF}}{60} \quad (16)$$

where C_E denotes carbon emission (KgCO₂), C_T is cutting time (min), and C_{EF} is the carbon emission factor, which is equal to 0.4261 KgCO₂/kWh (according to CO₂ database of Turkey grid electricity Transmission, February 2023).

Moreover, the materials removal rate (MRR = 1000 * V * f * d) was estimated in one pass for each tool utilizing the optimal variables. The MRR for turning 30 HRC hard workpieces was found for insert types 1, 2, and 3, estimated as 3500, 3600, and 3800 mm³/min, respectively. However, insert type 3 has an 8.57% higher MRR than insert type-1 and a 5.55% higher MRR than insert type-2. Therefore, insert type 3 was most suitable for mass production among the selected inserts. The obtained results are in good alignment with the previous study related to the hard turning^{98,99} According to energy consumption data, carbon emissions, and MRR, insert type-3 was the best of the three selected to achieve more sustainable hard machining.

Conclusions

This research equated the machining execution of three distinct cutting tools with the same tool geometry in turning medium-hardened AISI 4340 grade steel workpieces. Moreover, a novel hybrid optimization (TOPSIS-sine cosine algorithm) was employed to determine the optimal values of input variables and output responses. The key findings are illustrated below:

- Insert type-3 (TiCN-Al₂O₃-TiN) performed better in comparison to insert type-1 (TiN-TiCN-TiN) and insert type-2 (TiN-TiCN-TiN), while insert type-1 performance was superior to insert type-2.
- The Al₂O₃ coating layer in insert type-3 provided better wear resistance and less heat transfer in the substrate; thus, the performance of this insert was superior to that of other used inserts.
- Workpiece hardness was found to be the most vital input term, as all responses are greatly enhanced when hardness changes from 30 to 40 HRC.
- The highest resultant force was achieved when machining was done on the workpiece having maximum hardness (40 HRC) using maximum speed (235 m/min), while the minimal resultant force was seen when machining was performed on the machining was done on the workpiece having minimal hardness (30 HRC) using least speed (235 m/min),
- The largest Ra was found to be 1.546 μ m when machining was done on the workpiece having maximum hardness (40 HRC) using minimal speed (175 m/min), utmost feed (0.2 mm/rev), and moderate cutting depth of cut (0.3 mm).
- The minimal Ra was traced to be 0.312 μ m when the experiment was accomplished on the minimum workpiece hardness (30 HRC) with the shortest levels of input factors.
- The sound level in all studies was less than 85dB, indicating that the chosen cutting tools and process variables met environmental sustainability standards.

- The minimal power consumption for each tool was recorded at the lowest input level (a (mm)=0.2, f (mm/rev)=0.1, V (m/min)=175, and H (HRC)=30). It might be possible to remove the minimum workpiece hardness at the first cutting factor levels because of the lesser force required.
- Resultant force, power consumption, and sound level were increased with growing levels of cutting parameters, while surface roughness was significantly altered by the hardness of the workpiece, followed by tool feed.
- TOPSIS-Sine cosine algorithm, a hybrid optimization, was applied for multi-response optimization. The optimum level of input terms for insert type 1, 2, and 3 were found as follows: (a (mm)=0.2, f (mm/rev)=0.1, V (m/min)=175, and H (HRC)=30), (level (a (mm)=0.2, f (mm/rev)=0.1, V (m/min)=180, and H (HRC)=30), and (level (a (mm)=0.2, f (mm/rev)=0.1, V (m/min)=190, and H (HRC)=30), respectively.
- At optimal conditions, insert type-3 consumed 7.95% lower energy than type-1 and 5.33% lower than type-2. Similarly, insert type-3 produced 8.14% lower carbon emission at the same cutting conditions than type-1, while 5.39% lower than type-2. Therefore, it can be said that insert type-3 has better sustainability benefits than other types of inserts.
- At optimal conditions, insert type-3 has the highest metal removal rate (3800 mm³/min) in one pass turning of a 30 HRC hardness workpiece, followed by type-2 (3600 mm³/min) and insert type-1 (3500 mm³/min). Therefore, type-3 was more suitable for enhanced sustainability in medium-hard material machining.

Limitations and future scope

- In this research, we have used a workpiece hardness range of 30–40 HRC. Therefore, similar research is recommended for higher-hardness workpieces.
- Also, this research considered a lower range of cutting parameters; however, for better productivity, it should be examined at a higher range of these parameters. Cutting parameters range could be selected in a large range (a (mm): 0.4–1.2, f (mm/rev): 0.1–0.3, V (m/min): 200–300) to see their effect.
- The statistical analysis was not considered in the current research. Therefore, it can be considered in future research.
- The coating properties have significant effects on tool performance. Therefore, it is recommended that machining performance among different coating tools be compared in future studies.
- Future studies should consider tool wear and surface integrity assessment.
- In further study, *MRR* can be considered a performance criterion in process optimization.
- The current study can be explored under different cooling environments (dry, MQL, and nanofluid/hybrid nanofluids), and sustainability investigation can be included.

Data availability

The datasets used and/or analysed during the current study available from the corresponding author on reasonable request.

Received: 2 April 2025; Accepted: 16 June 2025

Published online: 02 July 2025

References

1. Chinchankar, S. & Choudhury, S. Machining of hardened steel—experimental investigations, performance modeling and cooling techniques: A review. *Int. J. Mach. Tools Manuf* **89**, 95–109 (2015).
2. Klocke, F., Brinksmeier, E. & Weinert, K. Capability profile of hard cutting and grinding processes. *CIRP Ann.* **54**(2), 22–45 (2005).
3. Kundrak, J. et al. Accuracy of hard turning. *J. Mater. Process. Technol.* **202**(1–3), 328–338 (2008).
4. Bartarya, G. & Choudhury, S. State of the art in hard turning. *Int. J. Mach. Tools Manuf* **53**(1), 1–14 (2012).
5. Goindi, G. S. & Sarkar, P. Dry machining: A step towards sustainable machining—Challenges and future directions. *J. Clean. Prod.* **165**, 1557–1571 (2017).
6. Mallick, R. et al. Current status of hard turning in manufacturing: Aspects of cooling strategy and sustainability. *Lubricants* **11**(3), 108 (2023).
7. Son, N. P. A comprehensive review on cutting tool material in hard turning performance. *Eng. Technol. J.* **09**, 3778 (2024).
8. Mia, M. & Dhar, N. R. Prediction of surface roughness in hard turning under high pressure coolant using Artificial Neural Network. *Measurement* **92**, 464–474 (2016).
9. Mia, M. & Dhar, N. R. Optimization of surface roughness and cutting temperature in high-pressure coolant-assisted hard turning using Taguchi method. *Int. J. Adv. Manuf. Technol.* **88**, 739–753 (2017).
10. Varadarajan, A., Philip, P. & Ramamoorthy, B. Investigations on hard turning with minimal cutting fluid application (HTMF) and its comparison with dry and wet turning. *Int. J. Mach. Tools Manuf* **42**(2), 193–200 (2002).
11. Das, A. et al. A comparison of machinability in hard turning of EN-24 alloy steel under mist cooled and dry cutting environments with a coated cermet tool. *J. Fail. Anal. Prev.* **19**, 115–130 (2019).
12. Zawada-Tomkiewicz, A. Analysis of surface roughness parameters achieved by hard turning with the use of PCBN tools. *Est. J. Eng.* **17**(1), 88 (2011).
13. Zare Chavoshi, S. & Tajdari, M. Surface roughness modelling in hard turning operation of AISI 4140 using CBN cutting tool. *Int. J. Mater. Forming* **3**, 233–239 (2010).
14. Aouici, H. et al. Analysis of surface roughness and cutting force components in hard turning with CBN tool: Prediction model and cutting conditions optimization. *Measurement* **45**(3), 344–353 (2012).
15. Yang, W. P. & Tarnag, Y. Design optimization of cutting parameters for turning operations based on the Taguchi method. *J. Mater. Process. Technol.* **84**(1–3), 122–129 (1998).
16. Rao, C., Rao, D. N. & Srihari, P. Influence of cutting parameters on cutting force and surface finish in turning operation. *Procedia Eng.* **64**, 1405–1415 (2013).
17. Bartarya, G. & Choudhury, S. Effect of cutting parameters on cutting force and surface roughness during finish hard turning AISI52100 grade steel. *Procedia CIRP* **1**, 651–656 (2012).
18. Abouelatta, O. & Madl, J. Surface roughness prediction based on cutting parameters and tool vibrations in turning operations. *J. Mater. Process. Technol.* **118**(1–3), 269–277 (2001).

19. Das, S. R., Panda, A. & Dhupal, D. Hard turning of AISI 4340 steel using coated carbide insert: Surface roughness, tool wear, chip morphology and cost estimation. *Mater. Today Proc.* **5**(2), 6560–6569 (2018).
20. Akbar, F. & Arsalan, M. Experimental investigation of uncoated, single layer, and multilayer-coated TiAlN/TiN tool inserts in dry orthogonal cutting of AISI/SAE 4140 alloy steel. *Proc. Inst. Mech. Eng. Part B J. Eng. Manuf.* **238**(1–2), 95–107 (2024).
21. Vignesh, S. & Devi, G. R. Performance analysis of novel TiN coated and uncoated carbide tool in CNC wet turning of super duplex stainless steel to minimize tool wear. *Mater. Today Proc.* **79**, 155–158 (2023).
22. Wagri, N. K. et al. Investigation on the performance of coated carbide tool during dry turning of AISI 4340 alloy steel. *Materials* **16**(2), 668 (2023).
23. Brito, R. F. et al. Analysis of contact thermal resistance and the use of coatings on heat transfer in cemented carbide metal cutting tools. *Rev. Gestão Soc. E Ambient* **18**(7), 1–19 (2024).
24. Saydakhmedov, R. & Kadirbekova, K. Composition and properties of wear-resistant coatings based on titanium carbide synthesized by the PVD method. In *AIP Conference Proceedings*. (AIP Publishing, 2023)
25. Dabees, S. et al. Characterization and evaluation of engineered coating techniques for different cutting tools. *Materials* **15**(16), 5633 (2022).
26. Li, Y. et al. Cutting performance evaluation of the coated tools in high-speed milling of AISI 4340 steel. *Materials* **12**(19), 3266 (2019).
27. Saikaew, C., Paengchit, P. & Wisitsoraat, A. Machining performances of TiN+ AlCrN coated WC and Al₂O₃+ TiC inserts for turning of AISI 4140 steel under dry condition. *J. Manuf. Process.* **50**, 412–420 (2020).
28. Asiltürk, I. & Akkuş, H. Determining the effect of cutting parameters on surface roughness in hard turning using the Taguchi method. *Measurement* **44**(9), 1697–1704 (2011).
29. Ambhore, N., Kamble, D. & Chinchani, S. Evaluation of cutting tool vibration and surface roughness in hard turning of AISI 52100 steel: An experimental and ANN approach. *J. Vib. Eng. Technol.* **8**(3), 455–462 (2020).
30. Kaladhar, M. Modeling and optimization for surface roughness and tool flank wear in hard turning of AISI 4340 steel (35 HRC) using TiSiN-TiAlN nanolaminate coated insert. *Multidiscip. Model. Mater. Struct.* **17**(2), 337–359 (2020).
31. Zheng, G. et al. Wear mechanisms of coated tools in high-speed hard turning of high strength steel. *Int. J. Adv. Manuf. Technol.* **94**, 4553–4563 (2018).
32. Sharma, N. & Gupta, K. Influence of coated and uncoated carbide tools on tool wear and surface quality during dry machining of stainless steel 304. *Mater. Res. Express* **6**(8), 086585 (2019).
33. Ulas, H. B. Experimental determination of cutting forces and surface roughness when turning 50CrV4 steel (SAE 6150) and modelling with the artificial neural network approach. *Trans. Indian Inst. Met.* **67**, 869–879 (2014).
34. Ginting, A. et al. The characteristics of CVD-and PVD-coated carbide tools in hard turning of AISI 4340. *Measurement* **129**, 548–557 (2018).
35. Szczotkarz, N. et al. Formation of surface topography during turning of AISI 1045 steel considering the type of cutting edge coating. *Adv. Sci. Technol. Res. J.* **15**(4), 253–266 (2021).
36. Kumar, R. et al. Comparative investigation towards machinability improvement in hard turning using coated and uncoated carbide inserts: Part I experimental investigation. *Adv. Manuf.* **6**, 52–70 (2018).
37. Roy, S. et al. Cutting tool failure and surface finish analysis in pulsating MQL-assisted hard turning. *J. Fail. Anal. Prev.* **20**, 1274–1291 (2020).
38. Suresh, R., Basavarajappa, S. & Samuel, G. Some studies on hard turning of AISI 4340 steel using multilayer coated carbide tool. *Measurement* **45**(7), 1872–1884 (2012).
39. Şahinoğlu, A. & Rafiqhi, M. Optimization of cutting parameters with respect to roughness for machining of hardened AISI 1040 steel. *Mater. Test.* **62**(1), 85–95 (2020).
40. Dash, L. et al. Machinability investigation and sustainability assessment in hard turning of AISI D3 steel with coated carbide tool under nanofluid minimum quantity lubrication-cooling condition. *Proc. Inst. Mech. Eng. C J. Mech. Eng. Sci.* **235**(22), 6496–6528 (2021).
41. Das, S. R., Panda, A. & Dhupal, D. Experimental investigation of surface roughness, flank wear, chip morphology and cost estimation during machining of hardened AISI 4340 steel with coated carbide insert. *Mech. Adv. Mater. Mod. Process.* **3**, 1–14 (2017).
42. Chinchani, S. & Choudhury, S. K. Experimental investigations to optimise and compare the machining performance of different coated carbide inserts during turning hardened steel. *Proc. Inst. Mech. Eng. Part B J. Eng. Manuf.* **228**(9), 1104–1117 (2014).
43. Thakur, A. & Gangopadhyay, S. Evaluation of micro-features of chips of Inconel 825 during dry turning with uncoated and chemical vapour deposition multilayer coated tools. *Proc. Inst. Mech. Eng. Part B: J. Eng. Manuf.* **232**(6), 979–994 (2018).
44. Mir, M. J. & Wani, M. Performance evaluation of PCBN, coated carbide and mixed ceramic inserts in finish-turning of AISI D2 steel. *J. Tribol.* **14**, 10–31 (2017).
45. Al Awadh, M. et al. Machinability comparison of TiCN-Al₂O₃-TiN, TiAlN-TiN, and TiAlSiN coated carbide inserts in turning hardened AISI 4340 steel using grey-crow search hybrid optimization. *Metals* **13**(5), 973 (2023).
46. Butt, M. M., Najjar, K. A. & Dar, T. H. Experimental evaluation of multilayered CVD-and PVD-coated carbide turning inserts in severe machining of AISI-4340 steel alloy. *J. Tribol.* **29**, 117–143 (2021).
47. Duc, P. M. et al. An experimental study on the effect of tool geometry on tool wear and surface roughness in hard turning. *Adv. Mech. Eng.* **12**(9), 1687814020959885 (2020).
48. Azaath, L. M., Mohan, E. & Natarajan, U. Effect of rake angle and tool geometry during machining process of AISI 4340 steel in finite element approach. *Mater. Today Proc.* **37**, 3731–3736 (2021).
49. Dogra, M., Sharma, V. & Dureja, J. Effect of tool geometry variation on finish turning—A review. *J. Eng. Sci. Technol. Rev.* **4**(1), 1 (2011).
50. Kambagowni, V., Chitla, R. & Challa, S. Determining the effect of material hardness during the hard turning of AISI4340 steel. *J. Inst. Eng. (India) Series D* **99**, 185–192 (2018).
51. Chinchani, S. & Choudhury, S. Evaluation of chip-tool interface temperature: Effect of tool coating and cutting parameters during turning hardened AISI 4340 steel. *Procedia Mater. Sci.* **6**, 996–1005 (2014).
52. Chinchani, S. & Choudhury, S. Effect of work material hardness and cutting parameters on performance of coated carbide tool when turning hardened steel: An optimization approach. *Measurement* **46**(4), 1572–1584 (2013).
53. Ji, R. et al. Machining performance of silicon carbide ceramic in end electric discharge milling. *Int. J. Refract. Metal Hard Mater.* **29**(1), 117–122 (2011).
54. Chi, Y. et al. Comparative study on machinability and surface integrity of γ -TiAl alloy in laser assisted milling. *J. Market. Res.* **33**, 3743–3755 (2024).
55. Tejani, G. G., Bhensdadia, V. H. & Bureerat, S. Examination of three meta-heuristic algorithms for optimal design of planar steel frames. *Adv. Comput. Des.* **1**(1), 79–86 (2016).
56. Mehta, P., Kumar, S. & Tejani, G. G. MOBBO: A multiobjective brown bear optimization algorithm for solving constrained structural optimization problems. *J. Optim.* **2024**(1), 5546940 (2024).
57. Mashru, N., Tejani, G. G. & Patel, P. Reliability-based multi-objective optimization of trusses with greylag goose algorithm. *Evol. Intel.* **18**(1), 25 (2025).
58. Mehta, P., Tejani, G. G. & Mousavirad, S. J. Structural optimization of different truss designs using two archive multi objective crystal structure optimization algorithm. *Sci. Rep.* **15**(1), 14575 (2025).

59. Adegboye, O. R. et al. Salp navigation and competitive based parrot optimizer (SNCPPO) for efficient extreme learning machine training and global numerical optimization. *Sci. Rep.* **15**(1), 13704 (2025).
60. Jagadish, Zindani, D., Selvam, A., Tejani, G. G. & Santhosh, A. J. Optimization of process parameter for green die sinking electrical discharge machining: A novel hybrid decision-making approach. *Sci. Rep.* **15**(1), 13489 (2025).
61. Anka, F., Tejani, G. G., Sharma, S. K. & Baljon, M. A bioinspired method for optimal task scheduling in Fog-Cloud environment. *Comput. Model. Eng. Sci.* **142**, 2691–2724 (2025).
62. Mirjalili, S. SCA: A sine cosine algorithm for solving optimization problems. *Knowl.-Based Syst.* **96**, 120–133 (2016).
63. Singh, P., Kottath, R. & Tejani, G. G. Ameliorated follow the leader: algorithm and application to truss design problem. *Structures* **2**, 181–204 (2022).
64. Hua, L., Du, Y., Qian, D., Sun, M. & Wang, F. Influence of prior cold rolling on bainite transformation of high carbon bearing steel. *Metall. and Mater. Trans. A.* **56**(2), 640–654 (2025).
65. Ren, Y. et al. Machine learning-based prediction of elliptical double steel columns under compression loading. *J. Big Data* **12**(1), 50 (2025).
66. Qian, Y. et al. Numerical characterization and formation process study of rail light bands in high-speed turnout areas. *Eng. Fail. Anal.* **168**, 109083 (2025).
67. Chen, R., Zeng, J., Yao, G. & Feng, F. Flow-stress model of 300M steel for multi-pass compression. *Metals* **10**(4), 438 (2020).
68. Wang, K. et al. Study on the damage mechanism of high-speed turnout switch rails on large ramps. *J. Central South Univ.* **32**(1), 288–303 (2025).
69. Shokoohi, Y., Khosrojerdi, E. & Shiadhi, B. R. Machining and ecological effects of a new developed cutting fluid in combination with different cooling techniques on turning operation. *J. Clean. Prod.* **94**, 330–339 (2015).
70. Öztürk, B. & Kara, F. Calculation and estimation of surface roughness and energy consumption in milling of 6061 alloy. *Adv. Mater. Sci. Eng.* **2020**, 1–12 (2020).
71. Kechagias, J. D. et al. A comparative investigation of Taguchi and full factorial design for machinability prediction in turning of a titanium alloy. *Measurement* **151**, 107213 (2020).
72. Alaba, E. et al. Evaluation of palm kernel oil as cutting lubricant in turning AISI 1039 steel using Taguchi-grey relational analysis optimization technique. *Adv. Ind. Manuf. Eng.* **6**, 100115 (2023).
73. Jagatheesan, K. & Babu, K. Taguchi optimization of minimum quantity lubrication turning of AISI-4320 steel using biochar nanofluid. *Biomass Convers. Biorefinery* **13**, 1–8 (2020).
74. Taka, M. et al. Selection of tool and work piece combination using multiple attribute decision making methods for computer numerical control turning operation. *Mater. Today Proc.* **4**(2), 1199–1208 (2017).
75. De, S. & Chakraborty, K. The machining parameter optimisation during the machining of the Cr-Mn austenitic stainless steel by the topsis method. *Mater. Today Proc.* **115**, 162–167 (2024).
76. Chakraborty, S. TOPSIS and Modified TOPSIS: A comparative analysis. *Decis. Anal. J.* **2**, 100021 (2022).
77. Govindaraju, K. & Sreenath, N. Hyperelliptic curve signcryption based privacy preserving message authentication and fuzzy TOPSIS-based trust management scheme for fog enabled VANET. *Int. J. Inf. Technol.* **17**(1), 247–261 (2025).
78. Kumar, B. P., Rao, P. S., Ravi Kiran, D. S. S., Venkatesh, D. J. & Rao, C. V. Parametric optimization of Al₂O₃-ZrO₂ (Y₂O₃) based self-lubricating composite cutting tool materials for turning operations using TOPSIS method. *Int. J. Interact. Des. Manuf. (IJIDeM)* **19**, 2727–2749 (2025).
79. Marxim Rahula Bharathi, B. et al. Unveiling optimal mother wavelets by COPRAS Method Analyzing speech signals despite face mask and shield obstacles. *Sci. Rep.* **15**(1), 14044 (2025).
80. Fahad, M., Mativenga, P. & Sheikh, M. An investigation of multilayer coated (TiCN/Al₂O₃-TiN) tungsten carbide tools in high speed cutting using a hybrid finite element and experimental technique. *Proc. Inst. Mech. Eng. Part B J. Eng. Manuf.* **225**(10), 1835–1850 (2011).
81. Bouacha, K. et al. Statistical analysis of surface roughness and cutting forces using response surface methodology in hard turning of AISI 52100 bearing steel with CBN tool. *Int. J. Refract Metal Hard Mater.* **28**(3), 349–361 (2010).
82. Demirpolat, H. et al. Comparison of tool wear, surface roughness, cutting forces, tool tip temperature, and chip shape during sustainable turning of bearing steel. *Materials* **16**(12), 4408 (2023).
83. Sk, T., Shankar, S. & Devendran, K. Tool wear prediction in hard turning of EN8 steel using cutting force and surface roughness with artificial neural network. *Proc. Inst. Mech. Eng. Part C J. Mech. Eng. Sci.* **234**(1), 329–342 (2020).
84. Abbas, A. T. et al. A closer look at precision hard turning of AISI4340: multi-objective optimization for simultaneous low surface roughness and high productivity. *Materials* **15**(6), 2106 (2022).
85. Agrawal, A. et al. Prediction of surface roughness during hard turning of AISI 4340 steel (69 HRC). *Appl. Soft Comput.* **30**, 279–286 (2015).
86. Bhuiyan, M. & Choudhury, I. 13.22—Review of sensor applications in tool condition monitoring in machining. *Compr. Mater. Process.* **13**, 539–569 (2014).
87. Özel, T., Hsu, T.-K. & Zeren, E. Effects of cutting edge geometry, workpiece hardness, feed rate and cutting speed on surface roughness and forces in finish turning of hardened AISI H13 steel. *Int. J. Adv. Manuf. Technol.* **25**, 262–269 (2005).
88. D'addona, D. & Raykar, S. J. Analysis of surface roughness in hard turning using wiper insert geometry. *Procedia CIRP* **41**, 841–846 (2016).
89. Özdemir, M. et al. Analysis and optimisation of the cutting parameters based on machinability factors in turning AISI 4140 steel. *Can. Metall. Q.* **61**(4), 407–417 (2022).
90. Rafiqhi, M. et al. Experimental assessment and topsis optimization of cutting force, surface roughness, and sound intensity in hard turning of AISI 52100 steel. *Surf. Rev. Lett.* **29**(11), 2250150 (2022).
91. Rafiqhi, M. The cutting sound effect on the power consumption, surface roughness, and machining force in dry turning of Ti-6Al-4V titanium alloy. *Proc. Inst. Mech. Eng. C J. Mech. Eng. Sci.* **236**(6), 3041–3057 (2022).
92. Şahinoğlu, A., Rafiqhi, M. & Kumar, R. An investigation on cutting sound effect on power consumption and surface roughness in CBN tool-assisted hard turning. *Proc. Inst. Mech. Eng. Part E J. Process. Mech. Eng.* **236**(3), 1096–1108 (2022).
93. Fink, D. J. *What is a Safe Noise Level for the Public?* 44–45 (American Public Health Association, 2017).
94. Kant, G. & Sangwan, K. S. Prediction and optimization of machining parameters for minimizing power consumption and surface roughness in machining. *J. Clean. Prod.* **83**, 151–164 (2014).
95. Nur, R. et al. Machining parameters effect in dry turning of AISI 316L stainless steel using coated carbide tools. *Proc. Inst. Mech. Eng. Part E J. Process. Mech. Eng.* **231**(4), 676–683 (2017).
96. Nur, R. et al. The effect of cutting parameters on power consumption during turning nickel based alloy. *Adv. Mater. Res.* **845**, 799–802 (2014).
97. Ross, N. S. et al. Carbon emissions and overall sustainability assessment in eco-friendly machining of Monel-400 alloy. *Sustain. Mater. Technol.* **37**, e00675 (2023).
98. Jacobson, M., Dahlman, P. & Gunnberg, F. Cutting speed influence on surface integrity of hard turned bainite steel. *J. Mater. Process. Technol.* **128**(1–3), 318–323 (2002).
99. Korkut, I. et al. Determination of optimum cutting parameters during machining of AISI 304 austenitic stainless steel. *Mater. Des.* **25**(4), 303–305 (2004).

Acknowledgements

The authors expressed their gratitude to Yozgat Bozok University, Yozgat, Turkey, for providing laboratory support to facilitate this research.

Author contributions

R.K-Writing – original draft M.R.—Resources O.I— Data Curation M.P.K.R- Formal analysis M. Ö- Writing review & editing S. Z- Writing review & editing A. P.- Project Administration R.S.- Optimization Algorithm and Project Supervision.

Funding

Open access funding provided by Manipal University Jaipur.

Declarations

Competing interests

The authors declare no competing interests.

Additional information

Correspondence and requests for materials should be addressed to A.P. or R.S.

Reprints and permissions information is available at www.nature.com/reprints.

Publisher's note Springer Nature remains neutral with regard to jurisdictional claims in published maps and institutional affiliations.

Open Access This article is licensed under a Creative Commons Attribution-NonCommercial-NoDerivatives 4.0 International License, which permits any non-commercial use, sharing, distribution and reproduction in any medium or format, as long as you give appropriate credit to the original author(s) and the source, provide a link to the Creative Commons licence, and indicate if you modified the licensed material. You do not have permission under this licence to share adapted material derived from this article or parts of it. The images or other third party material in this article are included in the article's Creative Commons licence, unless indicated otherwise in a credit line to the material. If material is not included in the article's Creative Commons licence and your intended use is not permitted by statutory regulation or exceeds the permitted use, you will need to obtain permission directly from the copyright holder. To view a copy of this licence, visit <http://creativecommons.org/licenses/by-nc-nd/4.0/>.

© The Author(s) 2025